



## Linking profiles of pathway activation with clinical motor improvements – A retrospective computational study

Konstantin Butenko<sup>a,b,\*</sup>, Ningfei Li<sup>b</sup>, Clemens Neudorfer<sup>b</sup>, Jan Roediger<sup>b,c</sup>, Andreas Horn<sup>b</sup>, Gregor R. Wenzel<sup>b</sup>, Hazem Eldebakey<sup>d</sup>, Andrea A. Kühn<sup>b</sup>, Martin M. Reich<sup>d</sup>, Jens Volkmann<sup>d</sup>, Ursula van Rienen<sup>a,e,f,\*</sup>

<sup>a</sup> Institute of General Electrical Engineering, University of Rostock, Rostock, Germany

<sup>b</sup> Movement Disorders and Neuromodulation Unit, Department for Neurology, Charité – Universitätsmedizin Berlin, Berlin, Germany

<sup>c</sup> Einstein Center for Neurosciences, Charité – Universitätsmedizin Berlin, Berlin, Germany

<sup>d</sup> Department of Neurology, University Hospital Würzburg, Würzburg, Germany

<sup>e</sup> Department Life, Light & Matter, University of Rostock, Rostock, Germany

<sup>f</sup> Department of Ageing of Individuals and Society, University of Rostock, Rostock, Germany

### ARTICLE INFO

#### Keywords:

Deep brain stimulation  
Pathway activation  
UPDRS-III score  
Pallidothalamic pathway  
Computational modeling  
Parkinson's disease

### ABSTRACT

**Background:** Deep brain stimulation (DBS) is an established therapy for patients with Parkinson's disease. *In silico* computer models for DBS hold the potential to inform a selection of stimulation parameters. In recent years, the focus has shifted towards DBS-induced firing in myelinated axons, deemed particularly relevant for the external modulation of neural activity.

**Objective:** The aim of this project was to investigate correlations between patient-specific pathway activation profiles and clinical motor improvement.

**Methods:** We used the concept of pathway activation modeling, which incorporates advanced volume conductor models and anatomically authentic fiber trajectories to estimate DBS-induced action potential initiation in anatomically plausible pathways that traverse in close proximity to targeted nuclei. We applied the method on two retrospective datasets of DBS patients, whose clinical improvement had been evaluated according to the motor part of the Unified Parkinson's Disease Rating Scale. Based on differences in outcome and activation levels for inpatient DBS protocols in a training cohort, we derived a pathway activation profile that theoretically induces a complete alleviation of symptoms described by UPDRS-III. The profile was further enhanced by analyzing the importance of matching activation levels for individual pathways.

**Results:** The obtained profile emphasized the importance of activation in pathways descending from the motor-relevant cortical regions as well as the pallidothalamic pathways. The degree of similarity of patient-specific profiles to the optimal profile significantly correlated with clinical motor improvement in a test cohort.

**Conclusion:** Pathway activation modeling has a translational utility in the context of motor symptom alleviation in Parkinson's patients treated with DBS.

### 1. Introduction

Deep brain stimulation (DBS) is an effective treatment for various neurological and mental disorders, and it has become an established therapy for patients suffering from therapy-refractory Parkinson's disease (PD). During DBS, short-duration high-frequency pulses are delivered to subcortical brain structures via implanted electrodes. These electrodes usually have 4 or 8 contacts, each of which can be used as a

current source. Modern DBS systems allow great flexibility in pulse modulation, including adjustment of width, amplitude, and frequency. Determining an optimal stimulation protocol in such a large parameter space is challenging, and to assist medical professionals in this procedure, *in silico* computational models for DBS could be of use (Frankemolle et al., 2010; Roediger et al., 2022; Vorwerk et al., 2019). Besides, such models could provide insights into the action mechanism of the treatment, which in turn could drive the development of more efficient and

\* Corresponding author.

E-mail addresses: [kbutenko@bwh.harvard.edu](mailto:kbutenko@bwh.harvard.edu) (K. Butenko), [ursula.van-rienen@uni-rostock.de](mailto:ursula.van-rienen@uni-rostock.de) (U. Rienen).

<https://doi.org/10.1016/j.nicl.2022.103185>

Received 11 April 2022; Received in revised form 27 July 2022; Accepted 2 September 2022

Available online 7 September 2022

2213-1582/© 2022 The Authors. Published by Elsevier Inc. This is an open access article under the CC BY-NC-ND license (<http://creativecommons.org/licenses/by-nc-nd/4.0/>).

effective stimulation paradigms.

In the basal ganglia, DBS has been hypothesized to create an “informational lesion” partly facilitated by electrical stimulation of highly excitable myelinated axons (Grill et al., 2004) that form projections across DBS targets, such as the subthalamic nucleus (STN) and the globus pallidus internus (GPi). To quantify the effect, different concepts have been proposed, among which the volume of tissue activated (Butson and McIntyre, 2005) or its approximations (Duffley et al., 2019) are most commonly employed. Multiple studies have investigated correlations of symptom alleviation with voxel metrics defined based on the volume of tissue activated and its interaction with structural and functional connectivity (Horn et al., 2017, 2019; Li et al., 2020; Middlebrooks et al., 2018). More recently, the concept of pathway activation modeling was proposed (Gunalan et al., 2017) that comprises advanced volume conductor models and anatomically authentic fiber trajectories to estimate a DBS-induced action potential initiation along pathways residing in the vicinity of the stimulation targets. To date, studies on Tourette syndrome, obsessive-compulsive disorder, treatment-resistant depression, and PD have successfully employed pathway activation modeling to estimate symptom alleviation in patients (Johnson et al., 2020; Hartmann et al., 2016; Howell et al., 2019; Gofdari et al., 2020). However, to our best knowledge, the method has not been applied on a cohort level to investigate correlations between DBS-induced activation, quantified using pathways composed of multiple axonal models, and alleviation of aggregated motor symptoms in PD.

In this retrospective computational study, we apply pathway activation modeling to identify the network correlates underlying the improvement of the Unified Parkinson’s Disease Rating Scale III score (motor examination, further referred to as UPRDS-III) and the Movement Disorder Society (MDS) sponsored revision of UPRDS-III in patients suffering from therapy-refractory PD. In particular, our aim is to evaluate the applicability of the analyzed modeling results for assessment of general alleviation of motor symptoms. We base this correlation model on pathway activation profiles defined by multiple pathways recruited by Subthalamic Nucleus Deep Brain Stimulation (STN-DBS). Correlating symptom alleviation with profiles instead of activation in individual pathways can be a more robust metric considering compensatory and adverse effects of fiber recruitment in the vicinity of the STN. Based on interprotocol scores, defined as the difference of two DBS-on UPDRS-III scores assessed in the training cohort for each patient, we construct a pathway activation profile theoretically leading to 100% UPDRS-III improvement from baseline and enhance it by analyzing the significance of activation levels in individual pathways. The performance of the resulting profile-based correlation model is then successfully tested in a held-out cohort.

## 2. Materials and methods

### 2.1. Patient cohorts and imaging

Two cohorts from independent DBS centers, namely Charité – Universitätsmedizin Berlin and Würzburg University Hospital, were retrospectively analyzed for derivation and validation of a pathway activation-based correlation model. The collection and analysis of all patient data from the training cohort was approved by the Local Ethics committee of Charité – Universitätsmedizin Berlin (master vote EA2/186/18). The collection and analysis of all patient data from the test cohort was approved by the institutional review board of the University Hospital of Würzburg (registration No. 150/15 amendment). The cohorts were formed based on the following criteria:

- availability of medical imaging data, such as preoperative T1-weighted magnetic resonance imaging (MRI) and postoperative computed tomography (CT), necessary for electrode localization and patient-specific modeling (see App. A: Suppl. 1 and Suppl. 2 for further details);

- current-controlled stimulation mode, which allows to compensate for a voltage drop on the electrode-tissue interface (Butson and McIntyre, 2005; Miocinovic et al., 2009; Butenko et al., 2022), reducing the computational model complexity;
- STN targeting via the dorsal portion of pallidus. The former restriction is imposed since only activation in pathways in the vicinity of the STN was investigated, and the latter criterion was applied to reduce effects of the pallidal lesioning.

As a result, 15 patients for the training (Berlin) and 19 for the test (Würzburg) cohort were admitted. Although the first cohort contained fewer patients, it provided a total of 30 datapoints: two stimulation protocols were documented on the same day for each patient as a part of another study that compared the standard of care with algorithm-guided DBS-programming, see (Wenzel et al., 2021) for further details. Later, this aspect was used to derive the correlation model. In both cohorts, the patients constituted a representative sampling of a clinical PD-DBS cohort (see Table 1). All received octopolar DBS electrodes bilaterally to STN (Fig. 1), either using omnidirectional or directional DBS electrodes (Boston Scientific Vercise™, Marlborough, MA, USA). Stimulation was performed using a conventional current-controlled DBS signal: a rectangular pulse of 20–60  $\mu$ s length, 79–185 Hz repetition rate, each followed by an extended charge balancing period at low amplitude (see App. A: Suppl. 1 and Suppl. 2 for further details). Motor performance in the training and the test cohorts was evaluated with either UPDRS-III or MDS-UPDRS-III, respectively. These scores are strongly ( $r > 0.95$ ) correlated (Merello et al., 2011), and, for brevity, both will be referred to as UPRDS-III. They were taken at baseline (off medication, DBS-off) preoperatively in the test cohort, and at least 6 months after surgery (same day as DBS-on scores) in the training cohort. UPDRS-III scores under active DBS (off medication) were acquired at least after 6 months in both cohorts.

Imaging data was processed using Lead-DBS software (Horn and Kühn, 2015; Horn et al., 2019) (lead-dbs.org), see Fig. 2. Postoperative volumes and preoperative weighted multimodal MRI scans were linearly co-registered using SPM12 (Friston et al., 1994) (fil.ion.ucl.ac.uk/spm). This was followed by a non-linear normalization step of co-registered patient scans to stereotactic Montreal Neurological Institute (MNI) space using Advanced Normalization Tools (ANTs, stnava.github.io/ANTs/) ‘Syn’ algorithm (Avants et al., 2008). We also accounted for potential non-linear displacements introduced by brain shift using an additional refinement of the co-registration step that focused on the subcortex. Electrodes were localized based on CT scans using PaCER (Husch et al., 2018), and results were visually evaluated and refined, if necessary.

Bioelectrical effects of DBS were modeled in patient-specific (native) space. To do so, patient-specific brain tissue distributions (grey matter, white matter and cerebrospinal fluid) were obtained by segmenting each patient’s individual MRI data using the Unified Segmentation approach as implemented in SPM12 (Ashburner and Friston, 2005). To account for tissue anisotropy, prominent along large fiber tracts, the mean diffusion tensor data of the human brain (Zhang and Arfanakis, 2018) were transformed into patient-specific space using the inverse deformation field derived from the diffeomorphic normalization procedure. The same procedure was applied to a basal ganglia pathway atlas (Petersen et al., 2019) that describes fiber distribution and classification necessary for pathway activation modeling. Created under the guidance of expert neuroanatomists, it provides an accurate description of axonal trajectories affected by STN stimulation. We must emphasize that these trajectories do not represent individualized tractography data, which can be extracted using various processing of diffusion imaging (Pujol et al., 2015). Instead, they stem from the atlas that defines thin bundles of the subcortex reconstructed based on MRI, histology, and relevant literature.

**Table 1**  
Cohort Demographics and Clinical Outcomes.

Cohort	No. (female)	Age, years	Disease duration, years	MDS-UPDRS-III Pre-op baseline	UPDRS-III Post-op baseline	(MDS-) UPDRS-III DBS-on Med-off
Training	15 (2)	62.4 ± 6.2	12.8 ± 4.8	—	40.6 ± 8.8	23.3 ± 8.7
Test	19 (7)	55.5 ± 5.7	9.8 ± 3.4	43.3 ± 9.4	—	22.3 ± 9.6

The training cohort was evaluated according to UPRDS-III (Unified Parkinson Disease Rating Scale, motor examination), and MDS-UPDRS-III (movement Disorder Society sponsored revision) was used in the test cohort; the scores are linearly dependent. Mean values ± standard deviations are reported. In the test cohort, baseline (off medication, DBS-off) was assessed preoperatively and in the training cohort at least 6 months after surgery. For each patient in the training cohort two stimulation protocols were documented: 21.5 ± 8.8 and 25.1 ± 8.3, respectively, with the score difference over the cohort 3.6 ± 7.3. Note that despite the age difference between the cohorts ( $t = 3.26$ ,  $p < 0.01$ ), there was no significant difference in gray matter-to-brain ratio ( $t = -0.22$ ,  $p = 0.82$ ), computed based on segmentations in native space.

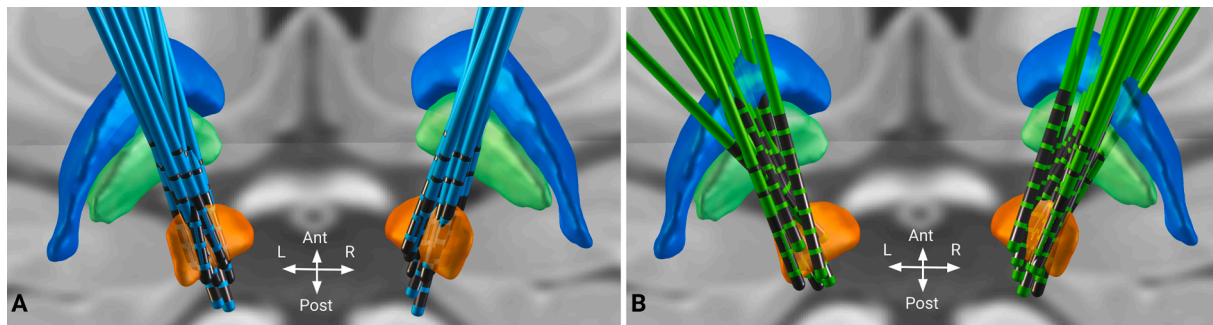


**Fig. 1.** Reconstruction of DBS electrodes in the training (Berlin, A) and the test (Würzburg, B) cohorts. Electrodes are visualized in standard stereotactic Montreal Neurological Institute (MNI) space using Lead-DBS. Displayed brain structures are defined by the DISTAL atlas (Ewert et al., 2018) and include subthalamic nucleus (orange), globus pallidus externus (blue) and globus pallidus internus (green). Note that the exact choice of the electrode placement depends on the patients' specific symptom profiles, anatomical variability (e.g. ventricle size, atrophy, asymmetry), and methodological limitations during image processing. Moreover, having distributed electrodes is beneficial when probing DBS effects on various neural substrates in the context of connectomic DBS.

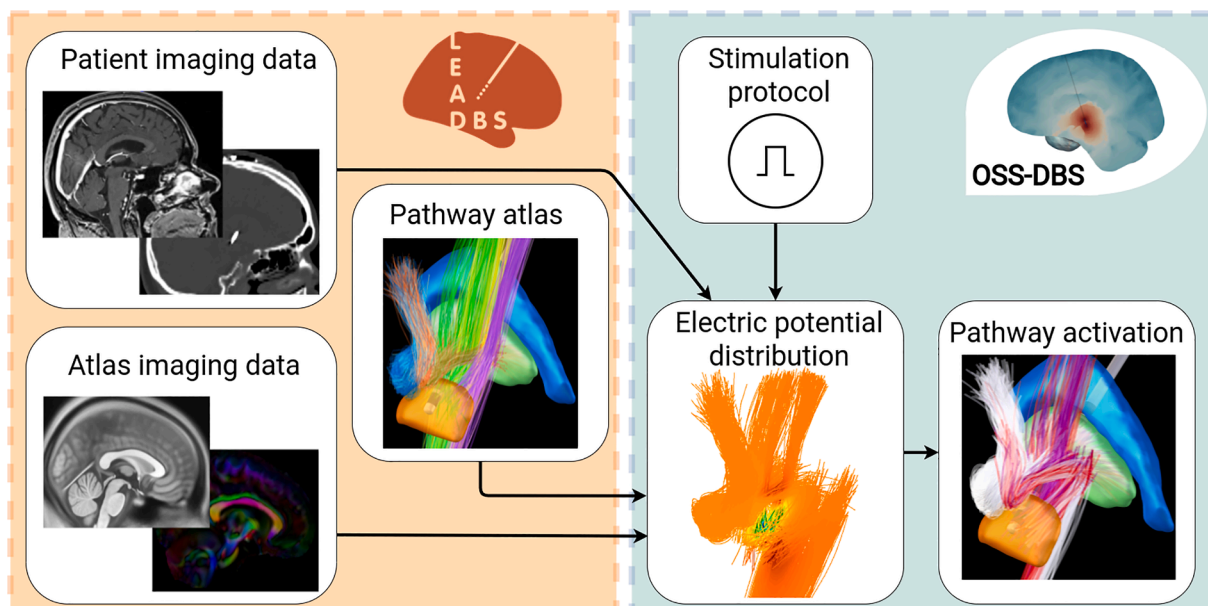


**Fig. 2.** Dataflow for computing pathway activation. Based on patient imaging and brain atlases, Lead-DBS (orange box) reconstructs the electrode and provides a description of tissue and water diffusion distributions in the brain. These data are used by OSS-DBS (green box) to create an accurate patient-specific volume conductor model. The model is then employed to compute electric potential distribution in space and time along axon models allocated on trajectories described by a pathway atlas. Finally, for the given distribution, the cable equation is solved to probe axonal activation, i.e. occurrence of an action potential in response to DBS.

## 2.2. Field and pathway activation modeling

Isotropic conductivity values for grey and white matter were evaluated in the frequency domain based on (Gabriel et al., 1996), but omitting  $\alpha$ -dispersion as proposed in Zimmermann and van Rienen (2021) and additionally upscaled. The conductivity  $\sigma$  of non-dispersive

cerebrospinal fluid was fixed to 2.0 S/m. In the power spectrum of a conventional DBS signal (up to 1 MHz), the conductivities were monotonically increasing ( $\sigma_{\text{grey}}$ : 0.168–0.235 S/m and  $\sigma_{\text{white}}$ : 0.120–0.153 S/m). To account for this dispersion, which was shown to affect the tissue-voltage response (Grant and Lowery, 2010), the Fourier Finite Element Method (Butson and McIntyre, 2005) was applied to solve the

quasistatic formulation of Maxwell's equations that describes the spatial distribution of the electric potential  $\phi(\mathbf{r})$ :

$$\nabla \cdot (\sigma(\mathbf{r}, \omega) \nabla \phi(\mathbf{r})) = 0, \quad (1)$$

where  $\omega = 2\pi f$  is the angular frequency of one of the harmonics that compose the DBS signal. Capacitive properties of brain tissue can be neglected in Eq. 1 due to its relatively low contribution after omitting  $\alpha$ -dispersion. An octave band approximation method (Butenko et al., 2019) was used to reduce the number of computations in the frequency domain. The solution in the time domain is then retrieved using an Inverse Fourier Transform. Anisotropy, especially prominent in white matter tracts (Geddes and Baker, 1967), was modeled by expressing conductivity in terms of tensors defined according to the mean diffusion tensor data that were normalized voxel-wise following the volume conservation approach (Güllmar et al., 2010) and scaled by the isotropic conductivity of brain tissue. The electrode-tissue interface was neglected assuming its minor effect on current-controlled stimulation (Butson and McIntyre, 2005) with a charge density per phase below  $0.03 \text{ mC/cm}^2$ . Nevertheless, the electrode's encapsulation layer was accounted for by removing axons within a 0.1 mm vicinity, where neuron degeneration and glial scarring occur. Note that although a 0.5 mm layer is often considered, it is not clear whether a substantial neuronal loss actually occurs that far from the electrode (Evers and Lowery, 2020). The accuracy of the Finite Element Method computations was controlled based on the convergence of the electric field and the current, and elements with large deviations were refined.

The obtained distribution of the extracellular potential in space and time was used to solve a double cable equation of a myelinated axon model described in McIntyre et al. (2002). The models were allocated on the trajectories delineated in Petersen et al. (2019) (for passing fibers, the closest point on the trajectory to active contacts was treated as the midpoint seed), and the pathway percent activation was computed as a fraction of axons in the pathway that elicited an action potential in response to the DBS pulse. In the present study, we modeled activation in the corticofugal pathway and its collateral to the STN, i.e. the hyperdirect pathway (HDP), originating in the primary and premotor cortex, as well as the supplementary motor area. To reduce the computational costs, the corticofugal pathway was uniformly down-sampled from 5000 to 1250 streamlines. In addition, activation in the pallidum subthalamic pathways (sensorimotor portion) and the pallidum thalamic pathways (ansa lenticularis and lenticular fasciculus) was investigated. Besides, we computed the extent of direct DBS recruitment of the passing cerebellothalamic tract associated with tremor suppression (Coenen et al., 2020). In total, 3500 axon models of 14 pathways per hemisphere were deployed for pathway activation modeling, with some axons being later removed due to their intersection with the electrode, the encapsulation layer or cerebrospinal fluid.

In the present study, the fiber diameters and the number of nodes of Ranvier, which together defined the axonal length, were fixed for axons within one pathway. A fiber diameter of  $3.0 \mu\text{m}$  was chosen for axons of the pallidum subthalamic projections with a length of 10 mm (35 nodes of Ranvier). For other pathways, the fiber diameter was set to  $5.7 \mu\text{m}$ . Note that these myelinated large caliber axons constitute a minority across the considered pathways (Liewald et al., 2014), but their activation might be of relevance in the context of high-frequency stimulation (Perge et al., 2012). The same axon model was employed in Howell et al. (2021), where it was noted that larger fiber diameters improve predictability of evoked potentials. In a preliminary analysis, we also tested a  $12.0 \mu\text{m}$  fiber diameter as suggested by the authors, but this setup yielded a high activation in the corticofugal pathway, which is unlikely for clinically accepted protocols due to evoked motor contractions. For computational reasons, the length of the axons of passage and the HDP was limited to 20 mm (40 nodes of Ranvier), thus not covering the whole length of the corresponding projections. Nevertheless, this truncation is acceptable due to a minor effect of DBS on distant axonal compartments,

and a preliminary analysis with longer axons yielded the same activation levels.

All steps described in this subsection were carried out using the open-source simulation software OSS-DBS (Butenko et al., 2020) that was developed for highly automated DBS modeling in heterogeneous anisotropic and dispersive volume conductor models. For the present study, the software was implemented as a computational backend, freely distributed along with Lead-DBS. The coupling allowed a seamless transition between state-of-the-art processing of medical imaging and accurate modeling of DBS-induced electric field with subsequent quantification of its effect on neural tissue using cable models. The OSS-DBS computations were encapsulated in Docker containers (docker.com/) deployed on Intel Xeon(R) Gold 6136 CPU @ 3.00 GHz x 48 cores with 376.6 GB of memory.

### 2.3. Analysis of pathway activation profiles

As a first exploratory step, we calculated correlations between activation levels of individual pathways and the UPDRS-III improvement from baseline in the training cohort. We employed the Pearson correlation coefficient, assuming a linear interaction between the quantities. The Spearman rank correlation was comparable for all tests presented in this study.

Secondly, we analyzed percent activation profiles  $\mathcal{A}$  (vector quantities composed of percent activation over 14 pathways) and their correlation with alleviation of motor symptoms. Since the training cohort contained two DBS-on datapoints per patient, we decided to use these measurements to derive a vector of the interprotocol UPDRS-III improvement in the pathway activation space (see Fig. 3). The difference in UPDRS-III scores between two protocols allowed us to compute a distance to a theoretical pathway activation profile of 100% improvement, i.e. an optimal percent activation profile:

$$\mathcal{A}_{\text{optimal}} = \mathcal{A}_+ + \frac{(\mathcal{A}_+ - \mathcal{A}_-)\text{UPDRS}_+}{\text{UPDRS}_- - \text{UPDRS}_+}, \quad (2)$$

where subscripts “+” and “-” refer to the better and the worse performing stimulation protocols, respectively. Such a definition of the optimal pathway activation profile is preferable over derivations using baseline, where only endogenous activity is present that is not quantified in the model and assumed to be overwritten by the DBS-induced activation of fiber tracts. If the score difference of the two protocols is small while their activation patterns are distinctly different, Eq. 2 diverges: two different solutions lead to a similar result. However, such divergent datapoints would have a very low normalized interprotocol improvement (a large change in activation leads to a low change in UPDRS-III, see the figure below, B), i.e. those datapoints are not informative.

The difference between two profiles was quantified with the Canberra distance (Lance and Williams, 1967)

$$d(\mathcal{A}_{\text{optimal}}, \mathcal{A}_a) = \sum_{i=1}^{14} w_i \frac{|\mathcal{A}_{\text{optimal},i} - \mathcal{A}_{a,i}|}{|\mathcal{A}_{\text{optimal},i}| + |\mathcal{A}_{a,i}|}, \quad (3)$$

where  $w_i$  is the weighting factor for the  $i$ -th pathway, whose default value is 1.0. The Canberra distance was chosen based on a preliminary analysis within the training cohort where it showed the highest performance in comparison with other metrics, such as Bray-Curtis dissimilarity and Euclidean distance. It is noteworthy that this normalized metric demonstrated the best performance, thus sparing us the argument of whether percent activation (percent of fibers activated in the tract) or absolute activation (total amount of fibers activated in the tract) should be employed when analyzing pathway activation results.

The next problem was to determine which patients, i.e. pairs of datapoints, to use for derivation of  $\mathcal{A}_{\text{optimal}}$ . At first glance, the patient with the best improvement between two DBS-on protocols would be a

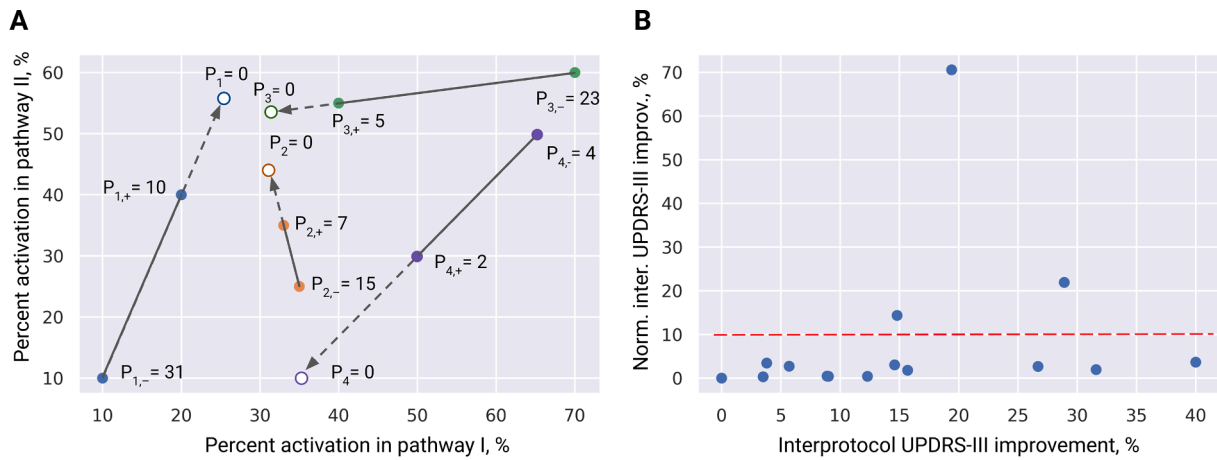


**Fig. 3.** Derivation of the optimal pathway activation profile. A: illustrative example of derivation using two DBS protocols per patient in a 2-D pathway activation space. Note that in our problem the space has 14 dimensions. Values of  $P_i$  denote the corresponding UPDRS-III scores for  $i$ -th patient, “+” and “-” subscripts refer to the more and less effective stimulation protocols, respectively. Divergent datapoints, i.e. those with a large difference in percent activation (a fraction of axons in the pathway that elicited an action potential in response to the DBS pulse) and small difference in motor improvement ( $P_4$  here), were not considered for the derivation of the optimal profile. B: the inpatient interprotocol UPDRS-III improvement in the training cohort with and without the normalization by the mean of percent activation differences. The normalized metric was used to select datapoints for the derivation of the optimal profile.

good candidate. However, the best improvement does not guarantee the shortest path to the optimal percent activation profile. Instead, we considered patients who had the highest interprotocol UPDRS-III improvement normalized by the mean of the difference vector ( $A_+ - A_-$ ). To increase the robustness of the correlation model,  $A_{optimal}$

can be averaged among several patients. In the present study, we picked three patients with a prominently higher normalized UPDRS-III improvement. Additionally, we tested the performance of  $A_{optimal}$  derived from all datapoints in the training cohort using a “leave-one-out” approach.

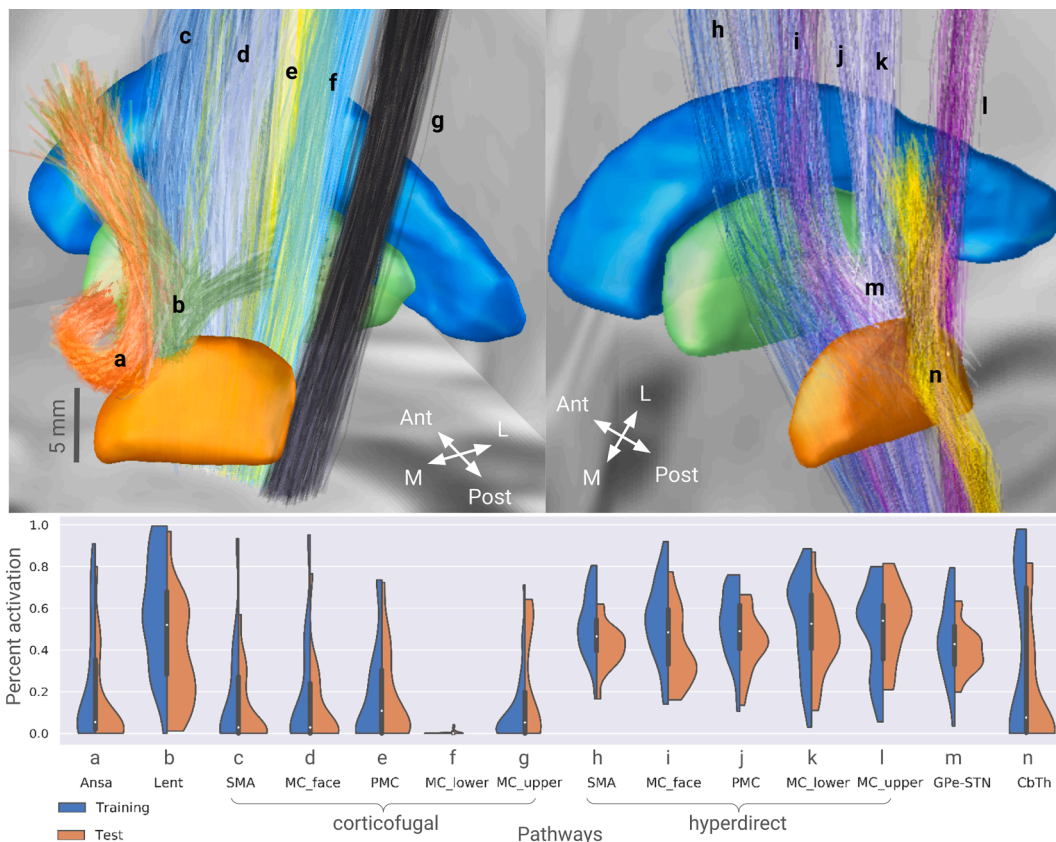


**Fig. 4.** Violin plots of pathway percent activation across both cohorts. The corresponding pathways are visualized in MNI space using Lead-DBS. Each plot contains 30 and 19 datapoints for the training and the test cohorts, respectively. MC and PMC refer to the primary and premotor cortical regions, SMA – supplementary motor area; cf and hdp are the corticofugal and the hyperdirect pathways, respectively; Ansa – ansa lenticularis, Lent – lenticular fasciculus, CbTh – cerebellothalamic pathway; l, f, up - lower extremity, face-neck region, and upper extremity in the primary motor cortex. Note that the cohorts’ datapoints provide comprehensive coverage of the pathway activation space.

Previous experimental and clinical studies showed that stimulation of specific pathways in the vicinity of the STN is associated with symptom alleviation and occurrence of side-effects (Sanders and Jaeger, 2016; Tommasi et al., 2008; Coenen et al., 2020; Chen et al., 2018; Irmen et al., 2020; Mosley et al., 2020). Therefore, we presume that the importance of matching the optimal profile is not uniform among pathways. To test this hypothesis, we optimized the weighting factor  $w_i$  for each pathway using the training cohort, but excluding those recruited for the derivation of  $\mathcal{A}_{\text{optimal}}$ . The optimization was conducted according to the following procedure. First, a patient was excluded, and the rest were randomly shuffled and split. Next, for one set, the weighting factors were optimized to maximize the inverse correlation of the Canberra distance and the UPDRS-III improvement, both from baseline and between protocols. The second set was then used to test the performance of the weighted metric. The procedure was repeated for all patients. Removal of a patient and random shuffling was employed to estimate convergence of the optimal weighting factors across the cohort, and multiple trials yielded no significant disparities introduced by the shuffling. Note that the limited number of datapoints overall necessitated use of the same patients (but in different combinations) in both sets.

### 3. Results

#### 3.1. Pathway activation and UPDRS-III improvement

Pathway percent activation computed for both cohorts are presented in Fig. 4 using violin plots that depict the kernel density estimation of the underlying distributions. Noteworthy is the difference in percent activation across the cohorts, which can be related to distinctions in the treatment strategies of the DBS centers. Analysis of activation in individual pathways and UPDRS-III improvement from baseline revealed only one pathway with a statistically significant positive correlation, namely, the HDP branch from the face-neck region of the primary motor cortex. However, the correlation was not significant in the test cohort.

The weak correlations for individual pathways might indicate an interplay of activation in different neural circuits.

Fig. 5, A shows activation profiles of the best responders, i.e. patients with the highest UPDRS-III improvement from baseline, and the theoretical 100% improvement profile, derived from datapoints of three patients (from the training cohort) with the highest normalized UPDRS-III improvement. The Canberra distance of the datapoints from the rest of the training cohort to the optimal profile showed a significant inverse correlation with the corresponding UPDRS-III improvements from baseline (see Fig. 6, A). In contrast, the optimal profile derived from all datapoints of the training cohort was not indicative (see App. B: Suppl. 1).

#### 3.2. Key pathways of the activation profile

Results of the optimization for the weighting factors  $w_i$  in the Canberra distance (see Eq. 3), conducted on datapoints of the training cohort, indicated that DBS-induced activation in specific pathways might play a prominent role in motor symptom alleviation (see Fig. 5).

In particular, the optimization emphasized a moderate activation in both pallidothalamic pathways as well as two branches of the HDP from the primary motor cortex, while avoiding stimulation of the corticofugal pathway descending from the supplementary motor area. Notably, the optimized weights were comparable over the optimization procedure (see Fig. 5, B) and were averaged to draw a general conclusion on the importance of particular pathways, where deviations in percent activation from the optimal profile led to worse performance. Fig. 6.

The averagely weighted Canberra distance to  $\mathcal{A}_{\text{optimal}}$  demonstrated a higher correlation with UPDRS-III improvement from baseline than the unweighted metric (Fig. 6, A), which is not, however, surprising, since the optimization was conducted on these datapoints. Therefore, the profile-based correlation model had to be validated on unseen patients from the held-out test cohort. Critically, patients from the test cohort did not play a role in the model selection process and were entirely naive to the final metric derived from the training cohort. This metric, the

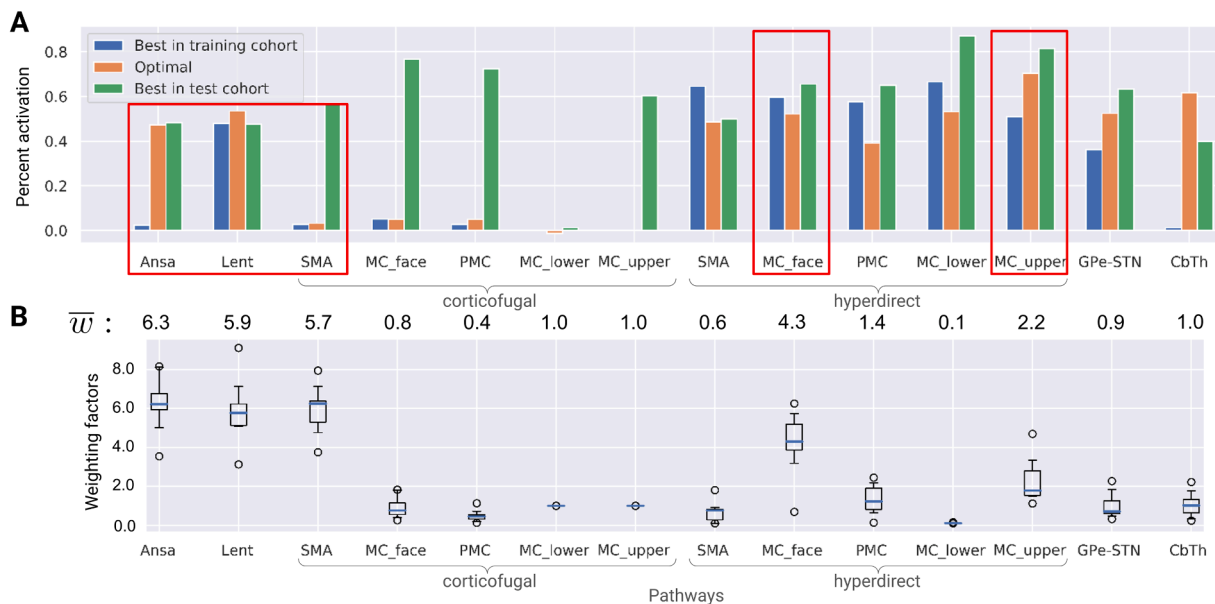


**Fig. 5.** Theoretical 100% UPDRS-III improvement optimal profile. MC and PMC refer to the primary and premotor cortical regions, SMA – supplementary motor area; cf and hdp are the corticofugal and the hyperdirect pathways, respectively; Ansa – ansa lenticularis, Lent – lenticular fasciculus, CbTh – cerebellothalamic pathway; l, f, up - lower extremity, face-neck region, and upper extremity in the primary motor cortex. A: percent activation for the optimal profile and the best responders from each cohort (should not be confused with the three patients that had the highest normalized interprotocol improvement). Note that the match between these datapoints and the optimal profile occurs for different pathways, suggesting that two distinct DBS mechanisms might be present. The mean values of optimized weighting factors below the bars can be interpreted as the importance of matching the optimal profile for a particular pathway. Red boxes highlight pathways with the highest effect on the correlation model. B: box plots of the optimized weighting factors computed with the 'leave-one-out' approach. Note the low number of outliers.

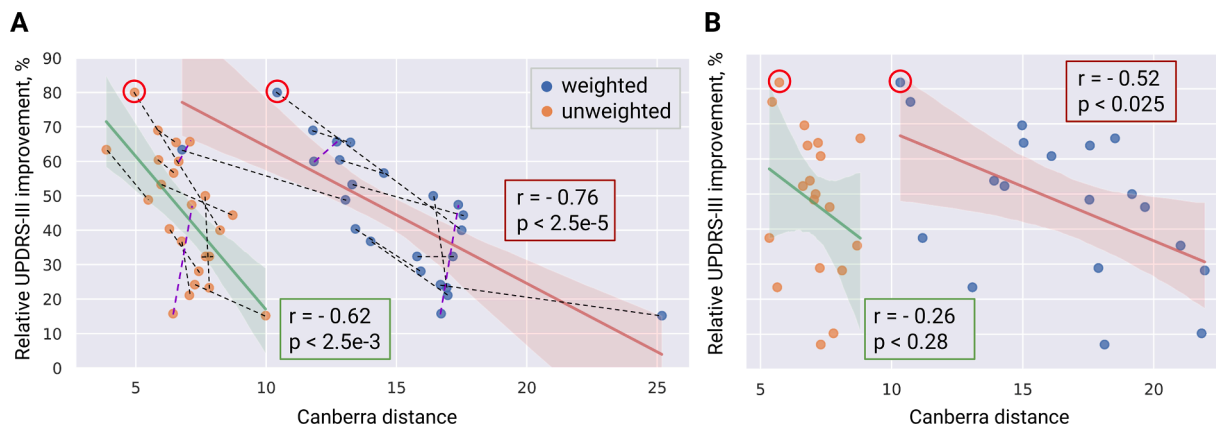


**Fig. 6.** Correlation of UPDRS-III improvement with weighted and unweighted Canberra distances to the optimal profile  $\mathcal{A}_{\text{optimal}}$ . The profile was defined in the pathway activation space based on three patients with the highest normalized interprotocol UPDRS-III improvement. The weighting of pathway contributions to the Canberra distances is determined using the rest of the training cohort. **A:** significant inverse correlations are observed in the training cohort whether with or without the weighting (the three patients used for derivation of  $\mathcal{A}_{\text{optimal}}$  are excluded). Dash lines between datapoints depict the interprotocol binary correlation (black – valid prediction, purple – false), the best responders from Fig. 5 are marked with red circles. **B:** in the held-out test cohort, only the weighted metric has a statistically significant correlation with UPDRS-III improvement.

weighted Canberra distance to  $\mathcal{A}_{\text{optimal}}$  defined in the training cohort, was inversely correlated with UPDRS-III improvement from baseline in patients of the test cohort, while the unweighted distance was not (see Fig. 6, B). Distribution of activation in the highly weighted pathways computed for the best responders is shown in Fig. 7. Furthermore, a sensitivity analysis was conducted for the percent activation in  $\mathcal{A}_{\text{optimal}}$ , and the results indicated robustness of the correlation model when using the weighted Canberra distance (see App. B: Suppl. 3).

#### 4. Discussion

In this study, we conducted pathway activation modeling for two cohorts of Parkinson's patients that underwent DBS surgery at two independent centers. Based on modeling results for a training cohort, we proposed a method to derive an optimal activation profile using differences in percent activation and UPDRS-III scores assessed for two protocols evaluated in each patient. Furthermore, we evaluated the importance of activation in particular pathways for the obtained profile.

At last, we demonstrated that proximity to the optimal activation profile in the multidimensional pathway activation space has a statistically significant correlation with UPDRS-III improvement in a test cohort from an independent center.

The methodology of optimal profile derivation, described in this study, required a comprehensive documentation of two distinct but clinically effective DBS-on Med-off protocols per patient. More often, only one protocol is available and hence replicating this exact analysis method is not possible in commonly available datasets. In our view, however, this highlights the unique value of acquiring datasets with multiple stimulation parameters tested in the same patient to construct meaningful models that are by design cleaned from a “patient factor”. In other words, this method allows to reduce the influence of the baseline “noise”, i.e. intrinsic activity not quantified in the model. In principle, the derived optimal profile should describe patient improvement in other centers based only on one protocol, as was demonstrated in this study for the test cohort from an independent DBS center. It should be noted that while the optimal profile was derived using only three

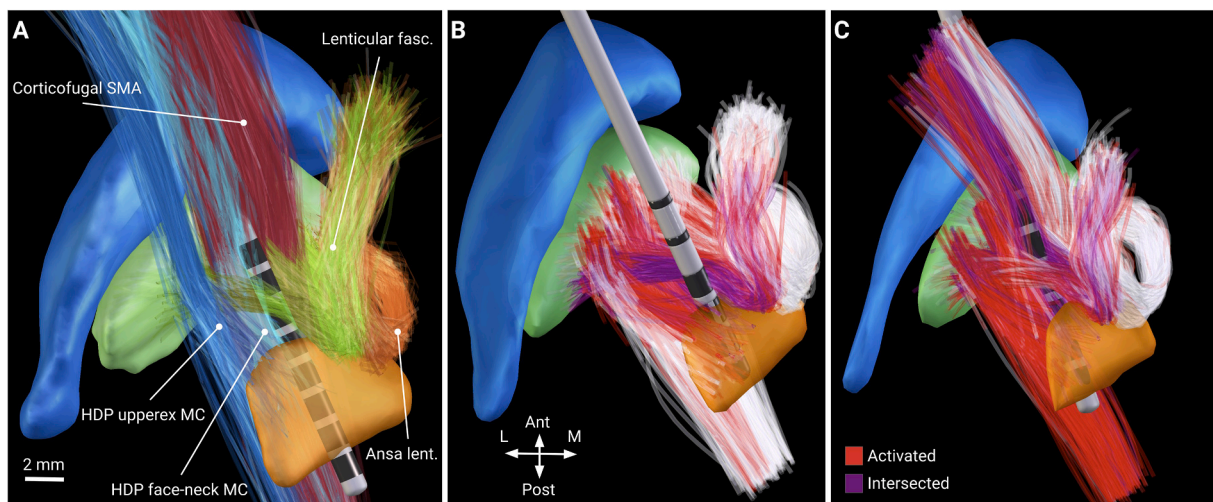


**Fig. 7.** Pathway activation visualized in Lead-DBS. **A:** pathways whose activation levels determine the UPDRS-III improvement (shown in MNI space). Cyan and blue – the hyperdirect pathway, descending from the face-neck and upper extremity of the primary motor cortex, red – the corticofugal pathway, descending from the supplementary motor area, green – lenticular fasciculus, orange – ansa lenticularis. **B** and **C:** pathway activation (shown on computational axon models in patient-specific space) for the best responders in the training and the test cohorts, respectively. Axons closer than 0.1 mm to the electrode are excluded (purple) due to presumable glial scarring and neurodegeneration. Note the high recruitment of the hyperdirect and the corticofugal pathway for the best responder in the test cohort.

patients who had a considerably higher normalized UPDRS-III improvement, the weighting factors of Canberra distances were defined using the rest of the training cohort.

#### 4.1. Effect of activation in individual pathways

Notably, the computed percent activation of individual axonal pathways demonstrated no clear correlation with clinical improvements. This result is especially remarkable for the hyperdirect pathway (HDP), associated with motor symptom alleviation in Parkinson's disease (PD) (Sanders and Jaeger, 2016; Chen et al., 2018; Li et al., 2014). Furthermore, even though activation in one branch of the HDP correlated with UPDRS-III improvement from baseline, the result was not reproducible in the test cohort. One possible explanation is that the correlation of improvement with HDP activation might be hindered by the nearby corticofugal pathway, whose stimulation has been associated with tetanic motor contractions (Tommasi et al., 2008). In addition, subthreshold stimulation of these tracts has been reported to exacerbate akinesia and bradykinesia (Xu et al., 2011), so patients may not necessarily show significant relief of motor symptoms despite high activation levels in the HDP. Admittedly, this was not the case for the best responder in the test cohort (see Fig. 5 and Fig. 7, C), possibly due to its individual lower responsiveness to the stimulation. We also analyzed correlations of UPDRS-III improvement with activation in the HDP, the corticofugal, and the pallidothalamic pathways without differentiating between branches. However, this did not yield conclusive results. It should be noted that the considered clinical DBS protocols did not produce motor contractions associated with a high activation in the corticofugal pathway, hence the effect could not be quantified in the correlation tests. Further studies are warranted to investigate pathway activation profiles associated with DBS-induced side-effects.

#### 4.2. Effect of balanced pathway activation

More conclusive results were obtained when considering motor improvement as a function of the whole activation profile. Defined by the weighted Canberra distance, discrepancy of test cohort profiles with the optimal percent activation profile demonstrated a statistically significant inverse correlation with UPDRS-III improvement from baseline. Importantly, the optimal profile was derived from datapoints of the training cohort, in particular, from differences of DBS-on inpatient UPDRS-III scores and corresponding percent activation.

When analyzing the optimal profile, it is notable that two branches of the HDP from the primary motor cortex and of the corticofugal pathway from the supplementary motor area were assigned high weighting factors (see Fig. 5, B), i.e. their percent activation was strongly associated with the motor outcome. For the corticofugal branch descending from the supplementary motor area, the percent activation in the optimal profile was minimal, suggesting its detrimental effect. On the other hand, the moderate percent activation in the presumably beneficial HDP branches can be explained by the proximity to the corticofugal pathway (note the high activation level of the HDP and the corticofugal pathway for the best responder in the test cohort).

The percent activation together with the weighting factors for the optimal profile could be used to hypothesize possible mechanisms of action of STN-DBS. Particularly high weights emphasize the importance of the pallidothalamic projections: the ansa lenticularis and lenticular fasciculus, which have been considered a functional continuum (Parent and Parent, 2004; Neudorfer and Maarouf, 2018). The latter factor is important when analyzing the activation profiles of the best responders. When comparing them to the weighted optimal profile, we can hypothesize that these pathways as well as the HDP are beneficial for alleviation of motor symptoms in PD. The ansa lenticularis and lenticular fasciculus are the primary inhibitory outputs of the basal ganglia to the ventral anterior thalamic nucleus (Lanciego et al., 2012), which itself is projecting to motor-relevant cortical regions. In a PD affected

network, the GPI exhibits bursting activity (Tachibana et al., 2011), which has been associated with generation of motor symptoms (Kim et al., 2017). Alleviation could arise from a direct modulation of this pathological activity, e.g. via an "informational lesion" induced by the non-physiological pattern of DBS (Grill et al., 2004). Furthermore, therapeutic effects of stimulation of the pallidothalamic pathways would also explain the comparable efficiency of GPI-DBS in treating motor symptoms of PD. In historical context of ablative surgery, lesioning of ansa lenticularis was shown to be beneficial for tremor alleviation (Wycis and Spiegel, 1952).

Considering these pathways as potential targets has important clinical implications. For DBS patients who respond poorly to the treatment, such as those in whom the active electrode contacts are outside the dorsolateral "sweet spot" of the STN (Dembek et al., 2019), clinicians could attempt to alleviate symptoms by thoroughly investigating stimulation responses for electrode contacts near the ansa lenticularis and lenticular fasciculus. Prospective studies could consider new implantation trajectories that allow both mechanisms with precise targeting of the hyperdirect and pallidothalamic pathways, preferably stimulated via different electrode contacts. This strategy would offer the possibility of inducing desynchronised DBS patterns.

At the same time, one should be aware that the STN is a site of convergence of different functional circuits (Accolla et al., 2016). That is a probable reason for its efficiency as a DBS target, where a simultaneous modulation of distinct symptoms is pursued. While detrimental effects could be associated with particular tracts, in this case, the corticofugal branch from the supplementary motor area (Fig. 5), it is of no surprise that the presented results do not pinpoint a particular neural pathway correlated with the UPDRS-III improvement. Instead, they suggest a profile of pathways whose balanced activation alleviates the profile of symptoms. Such a metric is more feasible than separately defined optimal activation levels, especially since pathway-specific DBS is not yet possible with clinically approved electrodes. While our results did not carve out a simple optimal activation profile, others have reported along the same lines that multiple small subcortical fibers seem to play a role for optimal DBS outcomes in PD (Noecker et al., 2021). Most tracts studied here have been considered to play a role in motor symptoms and our results suggest that it is not key to activate/modulate a single specific tract (such as the hyperdirect pathway alone) but instead a specific array of tracts connecting or passing the STN.

## 5. Limitations

Arguable results of the correlation tests for individual pathways might originate from uncertainties introduced by the computational model. We suspect that the lack of data on pathway-specific axonal morphology is the primary source of the error in pathway activation modeling. Furthermore, inaccuracies arise from volume conductor modeling, processing of medical images and clinical evaluation. In particular, the accuracy of the induced electric field distribution highly depends on the dielectric properties of brain tissue, subjected to uncertainties (McCann et al., 2019). Moreover, since these properties vary in space, accurate electrode reconstruction is crucial. Its accuracy is defined by multiple factors including patient imaging data, quality of co-registration and normalization, as well as accuracy of electrode artifact extraction from postoperative images. While reconstruction errors cannot be completely eliminated, Lead-DBS provides robust processing routines (Horn et al., 2019) and facilitates manual evaluation of intermediate results, yielding reliable electrode localizations. Variation in dielectric properties and neural morphology can be further addressed by means of uncertainty quantification, as was shown in Butenko et al. (2019) and Schmidt et al. (2013) in the context of DBS.

In the optimal profile, noteworthy is the small weighting factor of the sensorimotor pallidosubthalamic projections. That might be attributed to the limitations of the pathway activation modeling when investigating this local circuit, which excitatory-inhibitory reciprocity is a

probable source of synchronization in the basal ganglia (Nambu et al., 2015). Note that the subthalamic projections were not considered, since the electrodes are located near the cells of these afferents, and their stimulation might induce complex intrinsic dynamics not modeled in the study. Besides, due to the electrode implantation, these short pathways are relatively more exposed to glial scarring that potentially affects neurotransmission and extracellular ionic concentrations (Jakobs et al., 2019).

Apart from the limitations of the computational model the following study limitations deserve mentioning. First, not all efferent and passing pathways potentially affected by STN-DBS were modeled. To decrease the computational effort, we deliberately excluded the anterior cingulate and the prefrontal cortex assuming that they play a minor role in the motor symptoms of Parkinson's disease, although connectivity with the latter was associated with rigidity improvement (Akram et al., 2017). Among the local projections not examined, pathways of the substantia nigra pars reticulata are of particular interest, as it plays a similar role in the basal ganglia as the GPi. Unfortunately, these projections were not included in the basal ganglia pathway atlas (Petersen et al., 2019), employed here as an exclusive source of the structural connectivity.

Developed by experienced neuroanatomists using advanced visualization techniques, this atlas is less prone to contain false-positive trajectories occurring due to a poor signal-to-noise ratio of diffusion imaging, commonly employed for individualized fiber tractography. However, the atlas is neither patient-specific nor able to account for disease-related changes. In this study, individual anatomical variability was partially accounted for by translation of pathways to the patient-specific space using a subcortical normalization strategy (Ewert et al., 2019). Nevertheless, the proposed method of optimal activation profile derivation could be applied for basal ganglia pathways directly reconstructed from patient data as described in Pujol et al. (2017).

Furthermore, to generalize UPDRS-III improvement, we avoided differentiating between lateral and axial symptoms when analyzing activation levels, which were calculated separately for each hemisphere and then averaged. Differences in the pathway percent activation across both hemispheres are presented in App. B: Suppl. 2. In contrast to a symptom-circuit specific analysis, in this study we aimed at drawing a more general conclusion about therapeutic patterns for these representative cohorts of PD patients. Evidently, the circuit specificity could not be captured when analyzing complete UPDRS-III scores as was shown here by the absence of significant correlations between activation in individual pathways and the general improvement. Derivation of stimulation protocols for patient-specific needs in symptom alleviation is an important step in DBS advancement, and it is a subject of on-going research. However, low tremor levels in the recruited cohorts did not allow us to apply the proposed methodology to derive and compare activation profiles for hyperkinetic and hypokinetic aspects of PD.

Finally, the optimization procedure of the weighting factors, conducted in the training cohort, was developed rather intuitively, and future studies should consider more robust methods. It also remains unclear whether optimization should emphasize the interprotocol correlation of the improvement with the distance to the optimal profile or a general increase of correlation for all datapoints. For the given datapoints, we did not observe significantly higher correlations in the test cohort for either case.

## Funding

Funded by the Deutsche Forschungsgemeinschaft (DFG, German Research Foundation) – SFB 1270/1 – 299150580 and TRR 295 – 424778381. A.H. was further supported by the Deutsche Forschungsgemeinschaft (DFG, German Research Foundation) – Emmy Noether Stipend – 410169619 as well as Deutsches Zentrum für Luft- und Raumfahrt (DynaSti grant within the EU Joint Programme Neurodegenerative Disease Research, JPND). A.H. is participant in the BIH-Charité Clinician Scientist Program funded by the Charité –

Universitätsmedizin Berlin and the Berlin Institute of Health.

## CRediT authorship contribution statement

**K. Butenko:** Conceptualization, Methodology, Software, Investigation, Formal analysis, Visualization, Writing - Original Draft. **N. Li:** Methodology, Software, Validation, Writing - Review & Editing. **C. Neudorfer:** Formal analysis, Investigation, Writing - Review & Editing. **J. Roediger:** Resources, Investigation, Writing - Review & Editing. **A. Horn:** Conceptualization, Resources, Supervision, Writing - Original Draft. **G.R. Wenzel:** Resources, Writing - Review & Editing. **H. Eldabakey:** Resources, Writing - Review & Editing. **A.A. Kühn:** Resources, Project administration. **M.M. Reich:** Resources, Conceptualization, Writing - Review & Editing. **J. Volkmann:** Resources, Project administration. **U. van Rienen:** Resources, Supervision, Project administration, Funding acquisition, Writing - Review & Editing.

## Declaration of Competing Interest

J.V. have business relationships with Medtronic, Abbott, and Boston Scientific, which are makers of DBS devices, outside the submitted work. A.A.K. reports personal fees and non-financial support from Medtronic, personal fees from Boston Scientific, grants and personal fees from Abbott, outside the submitted work. M.R. reports grant support and honoraria for speaking from Medtronic and Boston Scientific, outside the submitted work. A.H. reports lecture fees for Medtronic and Boston Scientific and is a consultant for AlphaOmega. G.R.W received travel expenses and attendance fees by Boston Scientific and Ipsen Pharma. K. B., N.L., C.N., J.R., H.E. and U.v.R. have nothing to disclose.

## Appendix A. Supplementary data

Supplementary data associated with this article can be found, in the online version, at <https://doi.org/10.1016/j.nicl.2022.103185>.

## References

- Frankemolle, A.M.M., Wu, J., Noecker, A.M., Voelcker-Rehage, C., Ho, J.C., Vitek, J.L., et al., 2010. Reversing cognitive-motor impairments in Parkinson's disease patients using a computational modelling approach to deep brain stimulation programming. *Brain* 133 (3), 746–761. <https://doi.org/10.1093/brain/awp315>.
- Grill, W.M., Snyder, A., Miocinovic, S., 2004. Deep brain stimulation creates an informational lesion of the stimulated nucleus. *Neuroreport* 15, 1137–1140. <https://doi.org/10.1097/00001756-200405190-00011>.
- Butson, C., McIntyre, C.C., 2005. Tissue and electrode capacitance reduce neural activation volumes during deep brain stimulation. *Clin. Neurophysiol.* 116 (10), 2490–2500.
- Duffley, G., Anderson, D., Vorwerk, J., Dorval, A., Butson, C., 2019. Evaluation of methodologies for computing the deep brain stimulation volume of tissue activated. *J. Neural Eng.* 16 (6), 1–15.
- Horn, A., Reich, M.M., Vorwerk, J., Li, N., Wenzel, G., Fang, Q., et al., 2017. Connectivity predicts deep brain stimulation outcome in Parkinson disease. *Ann. Neurol.* 82 (1), 67–78. <https://doi.org/10.1002/ana.24974>.
- Horn, A., Wenzel, G., Irmen, F., Huebl, J., Li, N., Neumann, W.-J., et al., 2019. Deep brain stimulation induced normalization of the human functional connectome in Parkinson's disease. *Brain* 142 (10), 3129–3143. <https://doi.org/10.1093/brain/awz239>.
- Middlebrooks, E.H., Tuna, I., Grewal, S.S., Almeida, L., Heckman, M., Lesser, E., et al., 2018. Segmentation of the globus pallidus internus using probabilistic diffusion tractography for deep brain stimulation targeting in Parkinson disease. *Am. J. Neuroradiol.* 39 (6), 1127–1134. <https://doi.org/10.3174/ajnr.A5641>.
- Gunalan, K., Chaturvedi, A., Howell, B., Duchin, Y., Lempka, S., Patriat, R., et al., 2017. Creating and parameterizing patient-specific deep brain stimulation pathway-activation models using the hyperdirect pathway as an example. *PLoS ONE* 12 (4), 1–19.
- Johnson, K., Duffley, G., Foltynie, T., Hariz, M., Zrinzo, L., Joyce, E., et al., 2020. Basal ganglia pathways associated with therapeutic pallidal deep brain stimulation for Tourette syndrome. *Biological Psychiatry: Cognitive Neuroscience and Neuroimaging* 16 (10), 961–972. <https://doi.org/10.1016/j.bpsc.2020.11.005>.
- Hartmann, C.J., Lujan, J.L., Chaturvedi, A., Goodman, W.K., Okun, M.S., McIntyre, C.C., Haq, I.U., 2016. Tractography activation patterns in dorsolateral prefrontal cortex suggest better clinical responses in OCD DBS. *Front. Neurosci.* 9, 519. <https://doi.org/10.3389/fnins.2015.00519>.

- Howell, B., Choi, K.S., Gunalan, K., Rajendra, J., Mayberg, H.S., McIntyre, C.C., 2019. Quantifying the axonal pathways directly stimulated in therapeutic subcallosal cingulate deep brain stimulation. *Hum. Brain Mapp.* 40 (3), 889–903.
- Goftari, M., Kim, J., Johnson, E., Patriat, R., Palnitkar, T., Harel, N., 2020. Pallidothalamic tract activation predicts suppression of stimulation-induced dyskinesias in a case study of Parkinson's disease. *Brain Stimul.* 13 (6), 1821–1823. <https://doi.org/10.1016/j.brs.2020.09.022>.
- Miocinovic, S., Lempkam, S.F., Russo, G.S., Maks, C.B., Butson, C.R., Sakaie, K.E., Vitek, J.L., McIntyre, C.C., 2009. Experimental and theoretical characterization of the voltage distribution generated by deep brain stimulation. *Exp. Neurol.* 216 (1), 166–176. <https://doi.org/10.1016/j.expneurol.2008.11.024>.
- Butenko, K., van Rienen, U., 2022. Chapter 7 - dbs imaging methods iii: Estimating the electric field and volume of tissue activated. In: Horn, A. (Ed.), *Connectomic Deep Brain Stimulation*. Academic Press, pp. 147–168. <https://doi.org/10.1016/B978-0-12-821861-7.00021-X>.
- Vorwerk, J., Brock, A.A., Anderson, D.N., Rolston, J.D., Butson, C.R., 2019. A retrospective evaluation of automated optimization of deep brain stimulation parameters. *J. Neural Eng.* 16 (6) <https://doi.org/10.1088/1741-2552/ab35b1>.
- Wenzel, G., Roediger, J., Brücke, C., Marcelino, A., Gülke, E., Pötter-Nerger, M., et al., 2021. CLOVER-DBS: Algorithm-guided deep brain stimulation-programming based on external sensor feedback evaluated in a prospective, randomized, crossover, double-blind, two-center study. *J. Parkinson's Disease* 11 (4), 1887–1899. <https://doi.org/10.3233/JPD-202480>.
- Merello, M., Gerschovich, E.R., Ballesteros, D., Cerquetti, D., 2011. Correlation between the movement disorders society unified Parkinson's disease rating scale (MDS-UPDRS) and the unified Parkinson's disease rating scale (UPDRS) during l-dopa acute challenge. *Parkinsonism & Related Disorders* 17 (9), 705–707.
- Ewert, S., Plettig, P., Li, N., Chakravarty, M., Collins, D., Herrington, T., et al., 2018. Toward defining deep brain stimulation targets in MNI space: A subcortical atlas based on multimodal MRI, histology and structural connectivity. *NeuroImage* 170, 271–282.
- Horn, A., Kühn, A.A., 2015. Lead-DBS: A toolbox for deep brain stimulation electrode localizations and visualizations. *NeuroImage* 107, 127–135. <https://doi.org/10.1016/j.neuroimage.2014.12.002>.
- Horn, A., Li, N., Dembek, T., Kappel, A., Boulay, C., Ewert, S., et al., 2019. Lead-DBS v2: Towards a comprehensive pipeline for deep brain stimulation imaging. *NeuroImage* 184, 293–316.
- Friston, K.J., Holmes, A.P., Worsley, K.J., Poline, J.-P., Frith, C.D., Frackowiak, R.S.J., 1994. Statistical parametric maps in functional imaging: A general linear approach. *Hum. Brain Mapp.* 2 (4), 189–210. <https://doi.org/10.1002/hbm.460020402>.
- B. Avants, C. Epstein, M. Grossman, J. Gee, Symmetric diffeomorphic image registration with cross-correlation: Evaluating automated labeling of elderly and neurodegenerative brain. *Medical Image Analysis* 12 (1) (2008) 26–41, special Issue on The Third International Workshop on Biomedical Image Registration – WBIR 2006. doi: 10.1016/j.media.2007.06.004.
- Husch, A., Petersen, M.V., Gemmar, P., Goncalves, J., Hertel, F., 2018. PaCER - a fully automated method for electrode trajectory and contact reconstruction in deep brain stimulation. *NeuroImage: Clinical* 17, 80–89. <https://doi.org/10.1016/j.nicl.2017.10.004>.
- Ashburner, J., Friston, K.J., 2005. Unified segmentation. *NeuroImage* 26 (3), 839–851. <https://doi.org/10.1016/j.neuroimage.2005.02.018>.
- Zhang, S., Arfanakis, K., 2018. Evaluation of standardized and study-specific diffusion tensor imaging templates of the adult human brain: Template characteristics, spatial normalization accuracy, and detection of small inter-group FA differences. *NeuroImage* 172, 40–50. <https://doi.org/10.1016/j.neuroimage.2018.01.046>.
- Petersen, M.V., Mlakar, J., Haber, S., Parent, M., Smith, Y., Strick, P., et al., 2019. Holographic reconstruction of axonal pathways in the human brain. *Neuron* 104 (6), 1056–1064.e3. <https://doi.org/10.1016/j.neuron.2019.09.030>.
- Pujol, S., Wells, W., Pierpaoli, C., Brun, C., Gee, J., Cheng, G., et al., 2015. The DTI Challenge: Toward Standardized Evaluation of Diffusion Tensor Imaging Tractography for Neurosurgery. *J. Neuroimaging* 25 (6), 875–882. <https://doi.org/10.1111/jon.12283>.
- Gabriel, S., Lau, R., Gabriel, C., 1996. The dielectric properties of biological tissues: III. Parametric models for the dielectric spectrum of tissues. *Phys. Med. Biol.* 41 (11), 2271–2293. <https://doi.org/10.1088/0031-9155/41/11/003>.
- Zimmermann, J., van Rienen, U., 2021. Ambiguity in the interpretation of the low-frequency dielectric properties of biological tissues. *Bioelectrochemistry* 140, 107773. <https://doi.org/10.1016/j.bioelechem.2021.107773>.
- Grant, P.F., Lowery, M.M., 2010. Effect of dispersive conductivity and permittivity in volume conductor models of deep brain stimulation. *IEEE Trans. Biomed. Eng.* 57, 2386–2393.
- K. Butenko, C. Bahls, U. v. Rienen, Evaluation of epistemic uncertainties for bipolar deep brain stimulation in rodent models, in: 2019 41st Annual International Conference of the IEEE Engineering in Medicine and Biology Society (EMBC), 2019, pp. 2136–2140. doi:10.1109/EMBC.2019.8857910.
- Geddes, L., Baker, L., 1967. The specific resistance of biological material – A compendium of data for the biomedical engineer and physiologist. *Med. Biol. Eng.* 5, 271–293. <https://doi.org/10.1007/BF02474537>.
- Güllmar, D., Hauelsen, J., Reichenbach, J., 2010. Influence of anisotropic electrical conductivity in white matter tissue on the EEG/MEG forward and inverse solution. A high-resolution whole head simulation study. *NeuroImage* 51 (1), 145–163.
- Evers, J., Lowery, M., 2020. The Active Electrode in the Living Brain: The Response of the Brain Parenchyma to Chronically Implanted Deep Brain Stimulation Electrodes. *Operative Neurosurgery* 20 (2), 131–140. <https://doi.org/10.1093/ons/opa326>.
- McIntyre, C.C., Richardson, A.G., Grill, W.M., 2002. Modeling the excitability of mammalian nerve fibers: Influence of afterpotentials on the recovery cycle. *J. Neurophysiol.* 87 (2), 995–1006.
- Coenen, V.A., Sajonz, B., Prokop, T., Reisert, M., Piroth, T., Urbach, H., et al., 2020. The dentato-rubro-thalamic tract as the potential common deep brain stimulation target for tremor of various origin: an observational case series. *Acta Neurochir.* 162, 1053–1066.
- Liewald, D., Miller, R., Logothetis, N., Wagner, H.-J., Schüz, A., 2014. Distribution of axon diameters in cortical white matter: an electron-microscopic study on three human brains and a macaque. *Biol. Cybern.* 108, 541–557. <https://doi.org/10.1007/s00422-014-0626-2>.
- Perge, J.A., Niven, J.E., Mugnaini, E., Balasubramanian, V., Sterling, P., 2012. Why do axons differ in caliber? *J. Neurosci.* 32 (2), 626–638. <https://doi.org/10.1523/JNEUROSCI.4254-11.2012>.
- Howell, B., Isbaine, F., Willie, J.T., Opri, E., Gross, R.E., De Hemptinne, C., et al., 2021. Image-based biophysical modeling predicts cortical potentials evoked with subthalamic deep brain stimulation. *Brain Stimul.* 14 (3), 549–563. <https://doi.org/10.1016/j.brs.2021.03.009>.
- Butenko, K., Bahls, C., Schröder, M., Köhling, R., van Rienen, U., 2020. OSS-DBS: Open-source simulation platform for deep brain stimulation with a comprehensive automated modeling. *PLoS Comput. Biol.* 16 (7), 1–18.
- Lance, G., Williams, W.T., 1967. Mixed-data classificatory programs i - agglomerative systems. *Aust. Comput. J.* 1, 15–20.
- Roediger, J., Dembek, T.A., Wenzel, G., Butenko, K., Kühn, A.A., Horn, A., 2022. Stifit—a data-driven algorithm for automated deep brain stimulation programming. *Movement Disorders*. <https://doi.org/10.1002/mds.28878>.
- Sanders, T.H., Jaeger, D., 2016. Optogenetic stimulation of cortico-subthalamic projections is sufficient to ameliorate bradykinesia in 6-OHDA lesioned mice. *Neurobiol. Disease* 95, 225–237. <https://doi.org/10.1016/j.nbd.2016.07.021>.
- Tommasi, G., Krack, P., Fraix, V., Le Bas, J., Chabardes, S., Benabid, A., et al., 2008. Pyramidal tract side effects induced by deep brain stimulation of the subthalamic nucleus. *J. Neurol., Neurosurg. Psychiatry* 79 (7), 813–819.
- Chen, Y., Ge, S., Li, Y., Li, N., Wang, J., Wang, X., et al., 2018. Role of the cortico-subthalamic hyperdirect pathway in deep brain stimulation for the treatment of parkinson disease: A diffusion tensor imaging study. *World Neurosurgery* 114, e1079–e1085. <https://doi.org/10.1016/j.wneu.2018.03.149>.
- Irmen, F., Horn, A., Mosley, P., Perry, A., Petry-Schmelzer, J.N., Dafsari, H.S., Barbe, M., Visser-Vandewalle, V., Schneider, G.-H., Li, N., Kübler, D., Wenzel, G., Kühn, A.A., 2020. Left prefrontal connectivity links subthalamic stimulation with depressive symptoms. *Ann. Neurol.* 87 (6), 962–975. <https://doi.org/10.1002/ana.25734>.
- Mosley, P.E., Paliwal, S., Robinson, K., Coyne, T., Silburn, P., Tittgemeyer, M., Stephan, K.E., Perry, A., Breakspear, M., 2020. The structural connectivity of subthalamic deep brain stimulation correlates with impulsivity in Parkinson's disease. *Brain* 143 (7), 2235–2254. <https://doi.org/10.1093/brain/awaa148>.
- Lanciego, J.L., Luquin, N., Obeso, J.A., 2012. Functional neuroanatomy of the basal ganglia. *Cold Spring Harbor Perspectives in Medicine* 2 (12). <https://doi.org/10.1101/cshperspect.a009621>.
- Li, N., Baldermann, J., Kibleur, A., Treu, S., Akram, H., Elias, G., et al., 2020. A unified connectomic target for deep brain stimulation in obsessive-compulsive disorder. *Nature Commun.* 11 <https://doi.org/10.1038/s41467-020-16734-3>.
- Li, Q., Qian, Z.-M., Arbuthnot, G.W., Ke, Y., Yung, W.-H., 2014. Cortical Effects of Deep Brain Stimulation: Implications for Pathogenesis and Treatment of Parkinson Disease. *JAMA Neurol.* 71 (1), 100–103.
- Xu, W., Miocinovic, S., Zhang, J., Baker, K.B., McIntyre, C.C., Vitek, J.L., 2011. Dissociation of motor symptoms during deep brain stimulation of the subthalamic nucleus in the region of the internal capsule. *Exp. Neurol.* 228 (2), 294–297. <https://doi.org/10.1016/j.expneurol.2010.08.007>.
- Parent, M., Parent, A., 2004. The pallidofugal motor fiber system in primates. *Parkinsonism & Related Disorders* 10 (4), 203–211. <https://doi.org/10.1016/j.parkreldis.2004.02.007>.
- Neudorfer, C., Maarouf, M., 2018. Neuroanatomical background and functional considerations for stereotactic interventions in the H fields of Forel. *Brain Struct. Funct.* 223, 17–30. <https://doi.org/10.1007/s00429-017-1570-4>.
- Tachibana, Y., Iwamuro, H., Kita, H., Takada, M., Nambu, A., 2011. Subthalamo-pallidal interactions underlying parkinsonian neuronal oscillations in the primate basal ganglia. *Eur. J. Neurosci.* 34 (9), 1470–1484. <https://doi.org/10.1111/j.1460-9568.2011.07865.x>.
- Kim, J., Kim, Y., Nakajima, R., Shin, A., Jeong, M., Park, A.H., et al., 2017. Inhibitory basal ganglia inputs induce excitatory motor signals in the thalamus. *Neuron* 95 (5), 1181–1196.e8. <https://doi.org/10.1016/j.neuron.2017.08.028>.
- Wycis, H., Spiegel, E., 1952. Anotomy in paralysis agitans. *Confinia neurologica* 12 (4), 245–246. <https://doi.org/10.1159/000105783>.
- Dembek, T.A., Roediger, J., Horn, A., Reker, P., Oehr, C., Dafsari, H.S., et al., 2019. Probabilistic sweet spots predict motor outcome for deep brain stimulation in Parkinson disease. *Ann. Neurol.* 86 (4), 527–538. <https://doi.org/10.1002/ana.25567>.
- E.A. Accolla, M. Herrojo Ruiz, A. Horn, G.-H. Schneider, T. Schmitz-Hübsch, B. Draganski, A.A. Kühn, Brain networks modulated by subthalamic nucleus deep brain stimulation, *Brain* 139 (9) (2016) 2503–2515. doi:10.1093/brain/aww182.
- A.M. Noecker, A.M. Frankemölle-Gilbert, B. Howell, M.V. Petersen, S.B. Beylergil, A.G. Shaikh, et al., Stimvision v2: Examples and applications in subthalamic deep brain stimulation for parkinson's disease, *Neuromodulation: Technol. Neural Interface* 24 (2) (2021) 248–258. doi: 10.1111/ner.13350.
- McCann, H., Pisano, G., Beltrachini, L., 2019. Variation in reported human head tissue electrical conductivity values. *Brain Topogr.* 32 (5), 825–858.

- Schmidt, C., Grant, P., Lowery, M., van Rienen, U., 2013. Influence of uncertainties in the material properties of brain tissue on the probabilistic volume of tissue activated. *IEEE Trans. Biomed. Eng.* 60 (5), 1378–1387.
- Nambu, A., Tachibana, Y., Chiken, S., 2015. Cause of parkinsonian symptoms: Firing rate, firing pattern or dynamic activity changes? *Basal Ganglia* 5 (1), 1–6. <https://doi.org/10.1016/j.baga.2014.11.001>.
- Jakobs, M., Fomenko, A., Lozano, A.M., Kiening, K.L., 2019. Cellular, molecular, and clinical mechanisms of action of deep brain stimulation – a systematic review on established indications and outlook on future developments. *EMBO Mol. Med.* 11 (4), e9575 <https://doi.org/10.15252/emmm.201809575>.
- Akram, H., Sotiropoulos, S.N., Jbabdi, S., Georgiev, D., Mählknecht, P., Hyam, J., et al., 2017. Subthalamic deep brain stimulation sweet spots and hyperdirect cortical connectivity in Parkinson's disease. *NeuroImage* 158, 332–345.
- Ewert, S., Horn, A., Finkel, F., Li, N., Kühn, A.A., Herrington, T.M., 2019. Optimization and comparative evaluation of nonlinear deformation algorithms for atlas-based segmentation of DBS target nuclei. *NeuroImage* 184, 586–598.
- Pujol, S., Cabeen, R., Sébille, S.B., Yelnik, J., François, C., Fernandez Vidal, S., et al., 2017. In vivo exploration of the connectivity between the subthalamic nucleus and the globus pallidus in the human brain using multi-fiber tractography. *Front. Neuroanatomy* 10, 1–12. <https://doi.org/10.3389/fnana.2016.00119>.